# Characteristics of 4H-SiC and diamond detectors for direct fast neutron detection

Lei Ren [1, 2, #], Kai Su [3, 4, #], Yuncheng Han [1, †], Xiangdong Meng [1, 2], Wei Qian [1], Dan Xiao [1], Rui Zhang [1], Size Chen [1], Jie Shen [1], Gen Chen [1], Guoqiang Zhong [1], Jinfeng Zhang [3, 4], Yue Hao [3, 4], Jincheng Zhang [3, 4, †], Jie Yu [1]

1 Hefei Institutes of Physical Science, Chinese Academy of Sciences, Hefei, Anhui, 230031, China

2 University of Science and Technology of China, Hefei, Anhui, 230026, China

3 State Key Laboratory of Wide-Bandgap Semiconductor Devices and Integrated Technology, Faculty of Integrated Circuit, Xidian University, Xi'an, 710071, China

4 Xidian-Wuhu Research Institute, Wuhu, 241002, China

**# Equal contribution**

**† Corresponding author**

E-mail addresses: yuncheng.han@inest.cas.cn (Y. Han), jchzhang@xidian.edu.cn (J. Zhang)

## Abstract

Nuclear fusion research is regarded as a key direction for the development of future clean energy, and the precise detection of high-energy neutrons in high-temperature (up to 300°C) environments is particularly important to advance the technological realization of fusion reactors. 4H-SiC and diamond are ideal candidate materials for direct fast neutron detection in such conditions due to their high carbon content and wide-band gap properties. Device structure has great influence on the detection performance and high temperature performance of the detector. In this study, the detection performance of three kinds of detectors based on 4H-SiC and diamond (SiC-SBD, SiC-MSM and Diamond-MSM) under high temperature conditions was investigated, and the influence of device structure and semiconductor material on the high temperature performance was analyzed. The performance of these detectors was evaluated by comparing leakage current, energy resolution, and thermal stability. The results demonstrate that SBD devices exhibit relative better detection accuracy at temperatures below 150°C, but their performance significantly deteriorates as the temperature continue increases, while SiC-MSM shows superior high-temperature stability than SiC-SBD; additionally, Diamond-MSM achieved the best thermal stability over all the test temperature range. At 25℃-350℃, the leakage current of Diamond-MSM remains below 5 nA, while the energy resolution remains below 2.5%@5486 keV. In addition, Diamond-MSM also exhibits the best fast neutron response and excellent counting linearity. This work indicates the great potential of Diamond-MSM device for high-temperature detection applications in nuclear fusion research especially for high-temperature environments.

**Keywords:** 4H-SiC, Diamond, fast neutron detector, high temperature, energy resolution

## 1 Introduction

Nuclear fusion research is regarded as a key development direction for future clean energy, and precise detection of high-energy neutrons is crucial to advance the technological realization of fusion reactors [1]. CFETR (China Fusion Engineering Test Reactor), as a critical experimental platform, aims to study and validate various technologies for fusion reactors, which requires accurate detection of 14.1 MeV fast neutrons generated by fusion reactions under the harsh temperatures up to 300°C, in order to ensure the successful achievement of experimental objectives and deepen our understanding of fusion processes [2, 3].

Wide-band gap semiconductor materials have become an important choice in the field of fast neutron detection at high temperature due to their excellent performance in high temperature environments [4-6]. Direct detection of high-energy neutrons through nuclear reactions between elements in the material and neutrons has been proven to be an effective method for fast neutron detection. The carbon (C) element, due to its high cross-section with fast neutron and the distinct energy characteristics of its reaction products, plays a crucial role in high-energy neutron detection [7]. **Table 1** summarizes the main reaction types, cross-sections, and energy thresholds of carbon elements interaction with 14.1 MeV neutrons [8, 9], providing a theoretical foundation for efficient fast neutron detection. 4H-SiC and diamond, due to their high carbon content and wide-bandgap properties, are ideal materials for direct fast neutron detection in high-temperature environments [10, 11].

**Table 1** Main reactions between 14.1 MeV neutrons and carbon element

| Nuclear reaction | Cross section / mb | *Q* value / MeV | Energy threshold / MeV |
|---|---|---|---|
| $^{12}C$ (n, n) $^{12}C$ | 778.62 | 0.00 | 0.00 |
| $^{12}C$ (n, n′) $^{12}C$* | 210.60 | -4.44 | 4.81 |
| $^{12}C$ (n, n′) 3α | 200.00 | -7.37 | 8.43 |
| $^{12}C$ (n, $\alpha_0$) $^{9}Be$ | 62.30 | -5.70 | 6.42 |
| $^{12}C$ (n, $\alpha_1$) $^{9}Be$ | 20.30 | -7.38 | 8.09 |

In recent years, the application of 4H-SiC and diamond materials in fast neutron detection has been studied. In 2006, F. H. Ruddy prepared a fast neutron detector based on 4H-SiC, which realized the direct detection of 14.1 MeV fast neutrons [12]. In 2018, D. Rigamonti prepared the diamond single crystal detector grown by sCVD (standard Chemical Vapor Deposition), and realized the accurate detection of fast neutrons at normal temperature [13]. In 2018, O. Obraztsova compared the response of 4H-SiC and sCVD diamond-based detectors to 14-MeV neutrons, and both detectors showed well-characterized energy spectra for fast neutrons [14]. In 2016, D. Szalkai investigated the performance of 4H-SiC semiconductor detectors irradiated with 14 MeV fast neutrons at high temperatures (up to 500°C), and showed that thermal noise increased and the counting rate decreased as the temperature increased [15]. Although there has been some progress in the research, studies on fast neutron detection using carbon-based semiconductors in high-temperature environments remain limited.

The structural design of detectors plays a crucial role in determining their performance, particularly in terms of key parameters such as leakage current, energy

resolution, and thermal stability. The Metal-Semiconductor-Metal (MSM) structure is widely considered a classic design in diamond-based devices, primarily due to the challenges associated with P-type and N-type doping in diamond [16]. These doping processes are difficult to control in terms of concentration and efficiency, making the implementation of PN junctions challenging. Additionally, the metal-semiconductor contact in diamond is difficult to optimize, resulting in contact issues for SBD (Schottky barrier diodes), while heterojunction structures are also difficult to realize due to lattice mismatching and stress problems. Therefore, the MSM structure remains the preferred choice for diamond-based devices due to its simplicity and ease of fabrication. In contrast, 4H-SiC devices can be fabricated in various structures, such as SBD, PN, PIN, MOS (Metal-Oxide-Semiconductor), and MSM [17]. The SBD structure is particularly favored for its high energy resolution and fast response time among the various detector configurations [18]. In 2020, K. C. Mandal developed a Ni/4H-SiC SBD detector and reported an optimal energy resolution of 0.29% at 5486 keV based on 4H-SiC material [19]. However, there is still a lack of systematic comparison and in-depth research on which device structure and material can achieve high-performance fast neutron detection at high temperatures.

In this work, 4H-SiC detectors (with SBD and MSM structures) and diamond detector (with MSM structure) were design and fabricated. The influences of device structure and materials on detector performance have been characterized by comparing the detectors' critical parameters including leakage current, energy resolution and thermal stability under varying temperature environments for three different device groups. Additionally, their feasibility of directly detecting 14.1 MeV neutron were also explored.

## 2 Methods

### 2.1 Calculation methods

The I-V characteristics of Schottky diodes can be explained by thermionic emission model. A straight line fit to the ln($I$)–$V$ plot was used to determine the Schottky barrier height $\Phi_b$ (in volt) and ideality factor $n$ according to Eq. (1).

$$I_{SBD} = A A^{*} T^{2} \left(e^{-\frac{q \Phi_b}{k T}}\right)\left(e^{\frac{q V_d}{n k T}} - 1\right) \#(1)$$

where A is the device area, $A^{*}$ is the effective Richardson constant (146 A·cm$^{-2}$·K$^{-2}$ for 4H-SiC), k is the Boltzmann's constant, $T$ is the absolute temperature, q is the elementary charge of an electron, and $V_d$ is the applied reverse bias voltage.

The I-V characteristics of MSM devices can be explained by the following equation:

$$I_{MSM} \propto V_d \left(e^{-\frac{E_g}{k T}}\right) \#(2)$$

where $E_g$ is band gap width of semiconductor.

For the SBD junction, the width of depletion region can be estimated using the following formula:

$$W_d = \left[\frac{2\varepsilon_0\varepsilon_s(\Phi_b - V_d)}{qN_{eff}}\right]^{\frac{1}{2}} \#(3)$$

where $W_d$ is the width of depletion region, $\varepsilon_s$ is the relative dielectric constant of semiconductor, $\varepsilon_0$ is the vacuum permittivity, and $N_{eff}$ is the doping concentration.

The drift-diffusion model was applied to explain the role of charge collection efficiency (CCE) as a function of applying bias [10]:

$$CCE_{drift-diffusion} = \frac{1}{E_a}\int_0^{W_d}\left(\frac{dE}{dx}\right)dx + \frac{-}{E}$$

where $L_d$ is the minority carrier diffusion length, and for alpha particles $E_a$ is the energy, d$E$/d$x$ is the energy loss rate, and $L$ is the range, respectively.

The total number of nuclear reactions $R_t$ can be calculated by the following formula [22]:

$$R_t = \sum\varphi V_{det} \#(5)$$

where $\sum$ is the macroscopic cross section, $\varphi$ is the neutron fluence, $V_{det}$ is the effective volume of the detector.

The theoretical detection efficiency $\eta$ of neutron detectors based on 4H-SiC or diamond as a function of the semiconductor plate's thickness $L_m$, can be expressed in terms of the interaction probability as [23]:

$$\eta = 1 - e^{-\frac{L_m}{\lambda}} \#(6)$$

where λ, defined as $1/\sum$, represents the mean free path of the neutron.

The range and energy deposition of α particles in 4H-SiC and Diamond materials were calculated by simulation with the program of Stopping and Range of Ions in Matter (SRIM-2013) [24].

### 2.2 Device design and fabrication

From the ENDF/B-VIII.1 nuclear database, $^{12}C$ and $^{28}Si$ have a total reaction cross sections of 1.32 b and 1.89 b, respectively, for a neutron of 14.1 MeV [25]. The density of 4H-SiC is set as 3.2 g/cm$^3$, and the atomic nuclei of Si elements and C elements are both $4.81\times10^{22}$ cm$^{-3}$. The macroscopic cross section of 4H-SiC and 14.1 MeV neutrons is $1.54\times10^{-1}$ cm$^{-1}$, and the mean free path is 6.48 cm. The density of diamond is set as 3.5 g/cm$^3$, the nucleus density of C element is $1.76\times10^{23}$ cm$^{-3}$. The macroscopic cross section of diamond and 14.1 MeV neutron is $2.32\times10^{-1}$ cm$^{-1}$, and the mean free path is 4.30 cm.

According to Eq. (6), the ideal detection efficiency for 14.1 MeV neutrons dependent on thickness of 4H-SiC and diamond plates is calculated, as shown in **Fig. 1**. For both semiconductor plates, the detection efficiency increases approximately linearly over their thickness range of 0-1000 μm. Therefore, in order to improve the detection efficiency, the semiconductor plate thickness should be as high as possible, and the doping concentration should be reduced in order to improve the charge

collection efficiency. In this work, the detection efficiency of the detectors with 80-μm-thick 4H-SiC plate and 500-μm-thick diamond plate is calculated to be 0.12% and 1.17%, respectively.

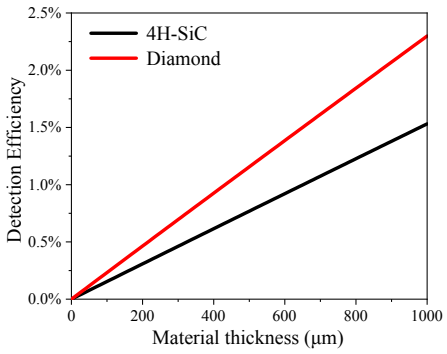


**Fig. 1** Detection efficiency of 4H-SiC and diamond plates for 14.1 MeV neutrons varies with their thickness

The 4H-SiC detector has been fabricated on a 4H-SiC $n^+$ substrate of 350-μm thickness, on which an 80-μm-thick n-type epitaxial layer with a low nitrogen doping concentration ~$7.1\times10^{13}$ $cm^{-3}$ was grown and used as the sensitive region. After the substrate cleaning using the standard Radio Corporation of America (RCA) procedure, Ti/Al/Ti/Au (30/30/30/30 nm) films were deposited onto the bottom side of 4H-SiC substrates via magnetron sputtering. These films were subsequently annealed at 500°C for 3 min in a nitrogen ($N_2$) atmosphere to form ohmic contacts. The Schottky electrode was prepared by Ni/Au (30/30 nm) films on the top of 4H-SiC epitaxial layer. For SiC-MSM detector, Ti/Au (30/30 nm) films were deposited at the top of 4H-SiC epitaxial layer and annealed at 400℃ in $N_2$ environment for 30 min.

The diamond detector was made in Xidian University. The single crystal diamond material was grown by microwave plasma chemical vapor deposition (MPCVD), and the detailed process method has been described in the reference [26]. Then, the diamond sample was soaked in $H_2SO_4$ for 30 minutes to remove amorphous carbon and organic contaminants. Afterward, the samples were subjected to ultrasonic cleaning in acetone, alcohol, and deionized water for 15 minutes each at 60 W power. Using electron beam evaporation and a metal mask, 150-nm-thick Au electrodes with dimensions of 3.6×3.6 $mm^2$ were deposited on both the top and bottom hydrogen terminated surfaces of the samples. The oxygen terminated surface were formed in the non-electrode region for electrical isolation. These similar device fabrication processes were described in our previous work [27, 28]. Subsequently, 200 nm-thick $Si_3N_4$ was deposited on both the top and bottom surfaces for surface passivation of the device using plasma-enhanced chemical vapor deposition (PECVD) at 350℃. The photolithography and inductively coupled plasma (ICP) etching processes are used to form electrical connection region pads. Then, the device was packaged in a TO-254 ceramic package using conductive silver paste (bottom surface) and silicon aluminum

wire (top surface). The Diamond-MSM detector was fabricated finally. The schematic diagram of the detectors used in this work are illustrated in **Fig. 2**.

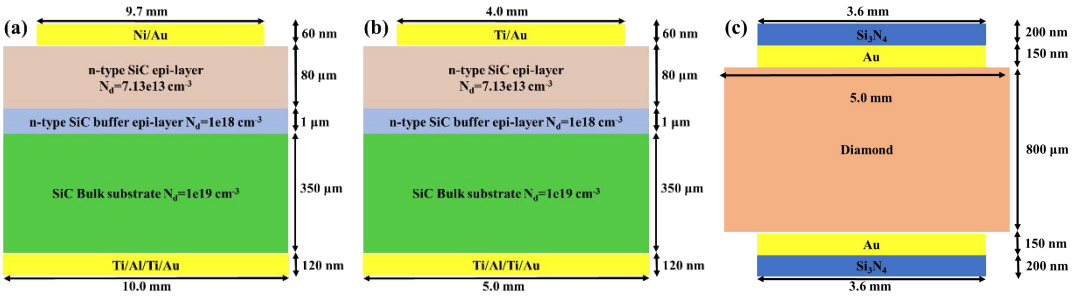


**Fig. 2** Schematic structure of (a) SiC-SBD; (b) SiC-MSM; (c) Diamond-MSM detector used in this study

## 2.3 Detector characterization

The basic electrical properties of the detectors were characterized through current-voltage (I–V) measurements. As shown in **Fig. 3**, the neutron test system employed in this study consists of the detector, a deuterium-tritium (D-T) neutron source, charge-sensitive preamplifiers, multichannel digital analyzers, and a Personal Computer running COMPASS software [10]. Neutron tests were conducted using the High Intensity Deuterium-Tritium Fusion Neutron Generator (HINEG), which generates $D^+$ ions via an Electron Cyclotron Resonance (ECR) ion source. D-T fusion neutrons are produced by bombarding a rotating tritium target with accelerated ions, resulting in a neutron yield of $2.0\times10^{10}$ n/s [29]. Signals from the neutron detectors were amplified using a multichannel charge-sensitive preamplifier (CSA). Data acquisition and analysis were performed using COMPASS software, which provided online operational control and data storage.

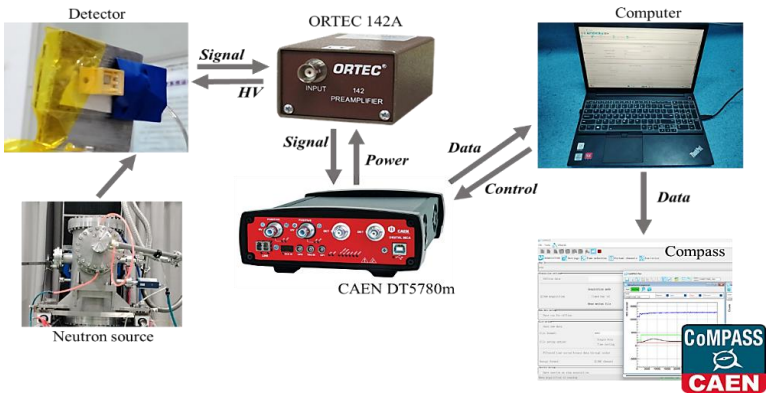


**Fig. 3** Schematic diagram of the data acquisition system for α energy spectrum measurements

## 3 Results and Discussion

### 3.1 Electrical characterization

**Fig. 4**(a) shows the forward I–V characteristic of SiC-SBD detector at 25℃ under dark conditions. Using the thermionic emission model, the barrier height $\Phi_b$ and ideality factor $n$ are calculated as 1.47 eV and 1.15, respectively. The reverse I-V

characteristics of the detector at different temperature were further characterized, and the results were shown in **Fig.** 4(b). At -200 V, the dark currents of SiC-SBD samples at 25℃, 100℃, 150℃ and 200℃ are 3.21 nA, 52.4 nA, 0.45 μA and 5.35 μA, respectively. The dark current of the SiC-SBD sample increases by about 1600 times from 25℃ to 200℃. It can be seen from Eq. (1) that the leakage current of the SBD device is strongly related to temperature T. At high temperatures, the increased thermal excitation of intrinsic carriers can lead to higher leakage currents, which may degrade the energy resolution and overall reliability of the detector [30]. In 2024, Norbert Gal developed a Ni/4H-SiC Schottky Barrier Diode (SBD) detector, which showed a leakage current of 1 pA at room temperature, increasing by a factor of 10000 to 10 nA at 500°C [31].

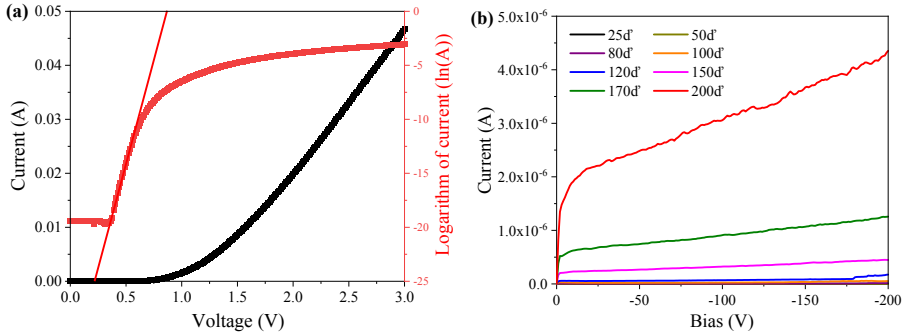


**Fig. 4** (a) Forward I−V characteristics at 25℃; (b) Reverse I−$V$ characteristics of the SiC-SBD detector at different temperatures

The dark current I-V characteristics of SiC-MSM detectors were measured at different temperatures, and the results were shown in **Fig.** 5. As expected, the dark currents increased with increasing temperature. At 200 V, the dark currents of SiC-MSM samples at 25℃, 50℃, 100℃, 150℃, 200℃, 250℃, 300℃ and 350℃ are 0.57 nA, 0.76 nA, 1.17 nA, 1.45 nA, 2.60 nA,8.59 nA, 16.14 nA and 91.75 nA, respectively. From 25℃ to 200℃, the leakage current of SiC-MSM device increases by about 4.5 times, and from 25℃ to 350℃, the leakage current increases by only about 161 times. Compared with SiC-MSM, the leakage current of SiC-SBD changes more drastically with temperature, which shows that there are significant differences between SiC-SBD and SiC-MSM in terms of internal physical mechanisms and structural responses to temperature elevation. The experimental results clearly show that SiC-SBD and SiC-MSM have completely different characteristics in terms of leakage current variation with temperature, which has important guiding significance for the applications of these two devices in different temperature environments. In high temperature environments, SiC-MSM has advantages over SiC-SBD due to their higher temperature stability and lower leakage current.

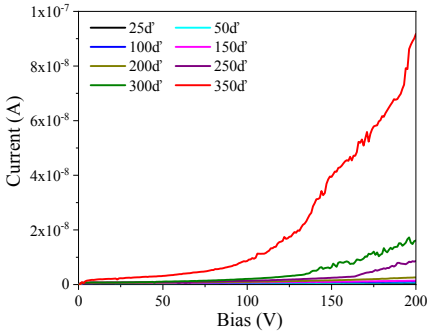


**Fig. 5** I-V characteristics measured for the SiC-MSM at different temperatures

The dark current I-V characteristics of Diamond-MSM devices were measured at different temperatures, and the results were shown in **Fig.** 6. At 200 V, the dark currents of Diamond-MSM samples at 25℃, 50℃,100℃, 150℃, 200℃, 250℃, 300℃ and 350℃ are 0.88 nA, 0.84 nA, 0.92 nA, 2.28 nA, 2.21 nA, 2.83 nA, 3.55 nA and 4.01 nA, respectively. Due to the higher band gap width of diamond, it can be seen that the leakage current increases from 0.88 nA to 4.01 nA at 25℃ to 350℃, which only increases by 4.5 times. In contrast to SiC-MSM, the dark currents of Diamond-MSM also generally rise with increasing temperature, yet the growth rate is not as significant as that of SiC-MSM. The reason for this lies in the fact that the bandgap of 4H-SiC is relatively narrow when compared with that of diamond. This implies that as the temperature increases, more electrons in 4H-SiC can be easily thermally excited to transition from the valence band to the conduction band, thereby making a more substantial contribution to the dark current. Due to the small growth of dark current and good stability at high temperatures, as well as the high thermal conductivity of diamond which enables effective heat dissipation and makes it less likely to be damaged by heat accumulation at high temperatures, Diamond-MSM is more suitable for high-temperature environments than SiC-MSM.

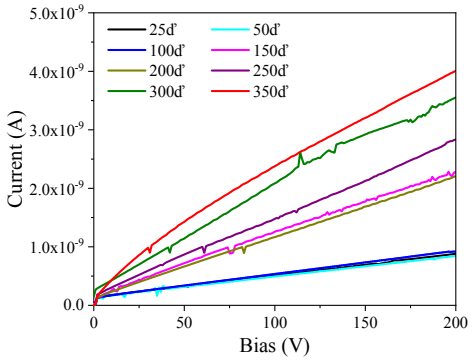


**Fig. 6** I-V characteristics of Diamond-MSM measured at different temperatures

### 3.2 Alpha response

Based on SRIM calculations, the ranges of 5486 keV alpha particles in 4H-SiC and diamond are 19 μm and 15 μm, respectively. This difference is mainly due to diamond having a higher density compared to 4H-SiC. **Fig.** 7 shows the final Bragg

ionization distribution for 4H-SiC and diamond. The corresponding d*E*/d*x* data will be used for subsequent CCE fitting calculations.

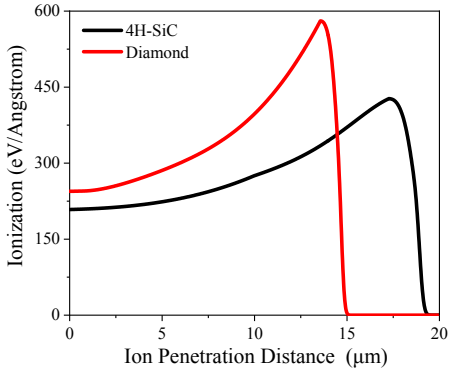


**Fig. 7** Bragg ionization curves of 5.486 MeV α ions in 4H-SiC and diamond

**Fig. 8**(a) shows the change of the detector's CCE and energy resolution with bias under the irradiation of an alpha particle source for SiC-SBD detector at room temperature. The experimentally obtained CCE data as a function of the reverse bias voltage can be well fitted by the theoretical CCE curve calculated by Eq. (4) with $L_d$ set as 13.5 μm. The overall CCE, especially at lower biases, is an interplay between the majority carrier (electron) drift and minority carrier diffusion. As the voltage increased, CCE reached saturation, and the energy resolution also reached the optimal working state, achieving an energy resolution of 0.61% at a -70 V bias. **Fig. 8**(b) presents the corresponding pulse height spectrum. All the three peaks corresponding to the primary alpha emissions $\alpha_1$, $\alpha_2$, and $\alpha_3$ with energies 5486, 5443, and 5388 keV, respectively, were clearly seen in both PHSs. It can be noted that the peak intensity ratio of $\alpha_1$, $\alpha_2$ and $\alpha_3$ is 85.23:12.67:0.94, which is basically consistent with the branching ratio of α-emission from $^{241}$Am source (86:12.5:1). The above results show that the SiC-SBD detector has excellent energy resolution and charge collection performance at room temperature.

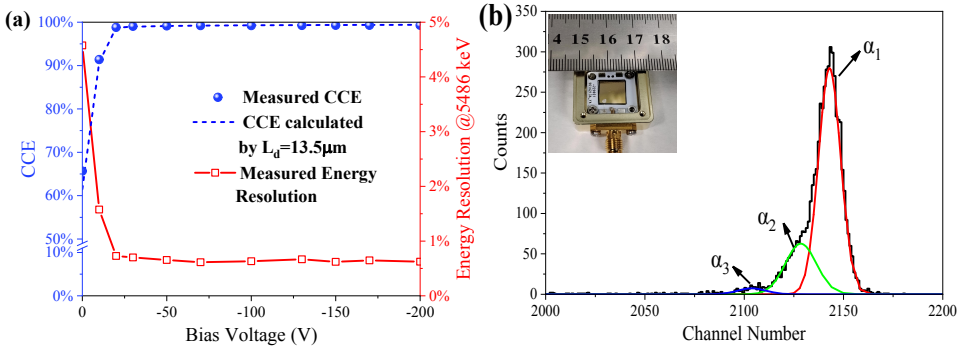


**Fig. 8** (a) The variation of CCE and energy resolution of SiC-SBD with bias voltage; (b) Corresponding PHS at -70 V

**Fig. 9**(a) shows the variation in CCE and energy resolution of the SiC-MSM detector as a function of bias voltage at room temperature. Notably, the detection of alpha particle signals is possible even at zero bias voltage. This can be attributed to the different diffusion lengths of electrons and holes within the detector. At zero bias, although no external electric field is applied, the charge carriers generated by the

alpha particles still have the ability to diffuse, so they can be collected without an external bias although with low efficient. When a bias is applied, the electric field leads to controllable drift of the charge carriers, aiding in their better collection in their life and leading to an increase in CCE. This is evident in the corresponding rise in the peak height of the alpha particle spectrum, where the alpha particle peak shifts towards higher channels with increasing bias voltage. This shift suggests that the detector performance is improved as the bias is increased, with a better energy resolution and more efficient charge collection.

It is important to note the fundamental differences in how MSM devices and SBD devices respond to applied bias voltage. In MSM devices, the application of bias voltage creates an electric field that sweeps the charge carriers (electrons and holes) towards the electrodes, facilitating signal generation. This process leads to a more efficient collection of charge carriers, which improves the detector's response. In contrast, in SBD devices, the application of bias voltage causes the depletion region to widen, which changes the way charge carriers are collected and results in a different effect on detector performance. The distinction between these two types of devices is crucial for understanding their respective responses to varying bias voltages, especially regarding the balance between signal sensitivity and resolution.

**Fig.** 9(b) presents the pulse height spectrum of SiC-MSM device obtained at a 200 V bias, showing an energy resolution of 1.21%. The alpha spectral lines from $^{241}$Am, specifically at 5.486, 5.443, and 5.388 MeV, overlap severely, resulting in a broad spectrum. This broadening can be attributed to the combined effects of electronic noise, imperfect charge collection, and the natural resolution limit of the detector. The FWHM of the spectrum at 200 V is 66.4 keV, which is significantly worse compared to the FWHM observed in SiC-SBD detector at -70 V. In fact, the energy resolution of the SiC-MSM detector is approximately twice that of SiC-SBD detector, indicating a clear performance deficit in terms of energy resolution.

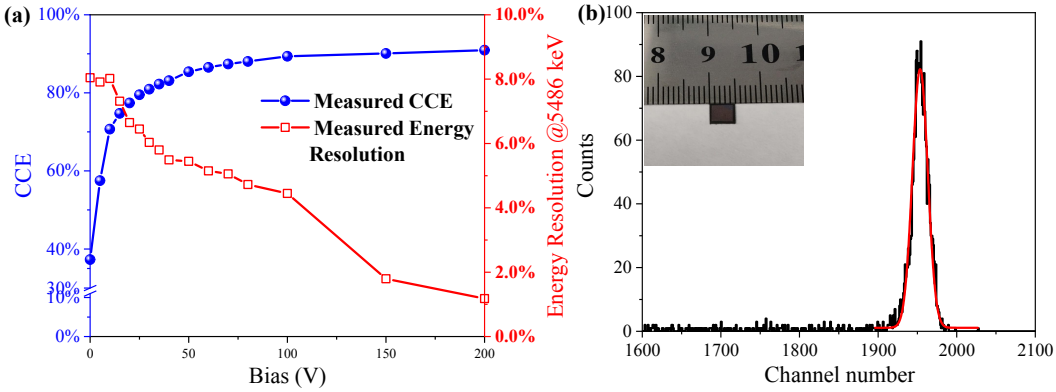


**Fig. 9** (a) Variation of CCE and energy resolution of SiC-MSM with bias voltage; (b) Corresponding PHS at 200 V

**Fig.** 10(a) shows the change of the CCE and energy resolution with bias for Diamond-MSM at room temperature. At zero bias, the alpha particle spectrum cannot be obtained, and it seems the alpha particle signals are lost in the bulk material of the detector. This is due to the lack of an electric field to collect the charge carriers

generated by the alpha particles at 0 V bias. To obtain meaningful data, different bias voltages above 30 V were applied. At higher bias voltages, the CCE increases, and the CCE improves with increasing bias voltage. This indicates that a stronger electric field helps collect more charge carriers generated by the incident alpha particles. The energy resolution also improves with increasing bias voltage, reaching its optimal value at 200 V. This is a common trend, where higher bias provides better charge separation and collection, leading to clearer peak detection. The pulse height spectrum as shown in **Fig.** 10(b) obtained at 200 V bias corresponds to an energy resolution of 0.97%. This level of resolution suggests that the detector can effectively distinguish between the energies of different alpha particles, with minimal uncertainty. The bias voltage affects both the charge collection efficiency and energy resolution. The results emphasize the importance of bias voltage in optimizing the performance of the Diamond-MSM detector. Both charge collection efficiency and energy resolution improve with the bias voltage, with the highest energy resolution of 0.97% at 200 V. This optimization is crucial for accurate alpha particle spectrum using this type of detector.

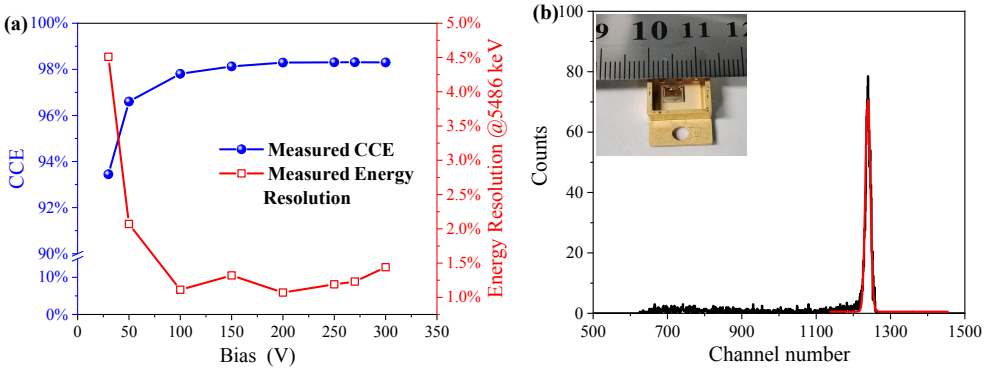


**Fig. 10** (a) The variation of CCE and energy resolution of Diamond-MSM with bias voltage; (b) Corresponding PHS at 200 V

**Fig.** 11(a) shows PHSs for the SiC-SBD detector when detecting 5.48 MeV $^{241}$Am alpha particles at different temperatures under a -70 V bias. As the temperature increases, the spectra broaden, and the peak height decreases, indicating a loss in signal clarity. **Fig.** 11(b) shows the energy resolution and the variation of the peak location with temperature over a range of 50°C to 200°C. A comparison of **Fig.** 11(b) and **Fig.** 4(b) reveals that the trend of energy resolution with temperature follows a similar pattern to that of the detector's leakage current with temperature. As the temperature rises, the leakage current increases, which leads to higher thermal noise in the detector. This increased noise contributes to the deterioration in energy resolution. At 200°C, the energy resolution of the SiC-SBD detector is 5.1%, a noticeable decline from its performance at lower temperatures. The increased leakage current and thermal noise interfere with the detector's capability to clearly distinguish between signals, broadening the spectral peaks and making precise energy measurement difficult. The worsening of energy resolution at higher temperatures limits the SiC-SBD detector in accurate alpha particle detection at elevated temperatures. At 200°C, the detector can no longer provide reliable alpha particle

detection. These results emphasize the importance of controlling temperature in the operation of SiC-SBD detectors, as elevated temperatures can significantly degrade their performance.

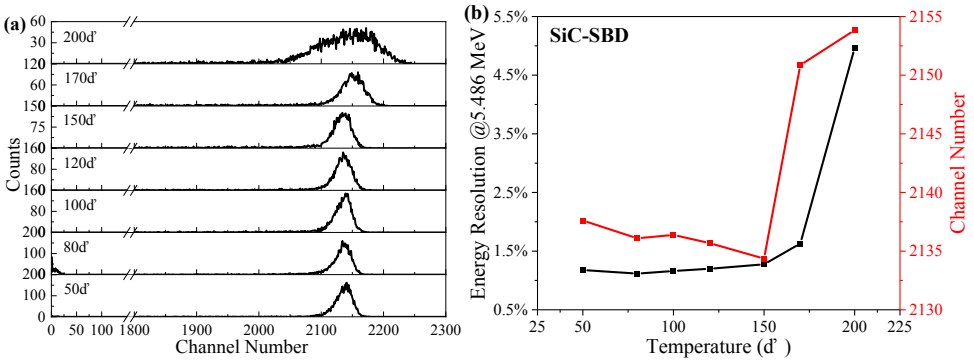


**Fig. 11** (a) PHSs of SiC-SBD at 50℃-200℃; (b) Energy resolution and peak position change with temperatures

The PHSs for the SiC-MSM detector detecting 5.48 MeV $^{241}$Am at different temperatures are shown in **Fig.** 12(a). The energy resolution and peak position vs. temperature curves are presented in **Fig.** 12(b) for temperatures ranging from 50°C to 350°C. The energy resolution is optimal at 120℃, which is due to the following reasons. Firstly, at 120°C, the leakage current is measured at 0.76 nA, which has minimal impact on broadening the energy spectrum, allowing for a more precise measurement. Secondly, temperature effects lead to a decrease in the average ionization energy of 4H-SiC, which explains the improvement in peak position from 50°C to 250°C. The decrease of ionization energy produces more electron hole pairs, reduces the energy spectrum broadening due to statistical fluctuations, and improves the energy resolution. However, as the temperature increases beyond 250°C, specifically at 270°C and 300°C, the operating voltage is reduced to 170 V and 150 V, respectively, to stabilize the baseline. This reduction in voltage leads to a drop in the peak intensity, as the applied bias is lower, affecting the overall detector performance. Despite these challenges, the SiC-MSM detector demonstrates higher thermal stability than the SiC-SBD detector, as the leakage current in SiC-MSM is better controlled across a broader temperature range. This indicates that SiC-MSM detectors may be more reliable for high-temperature applications compared to SiC-SBD detectors, making them better suited for environments with fluctuating or high temperatures.

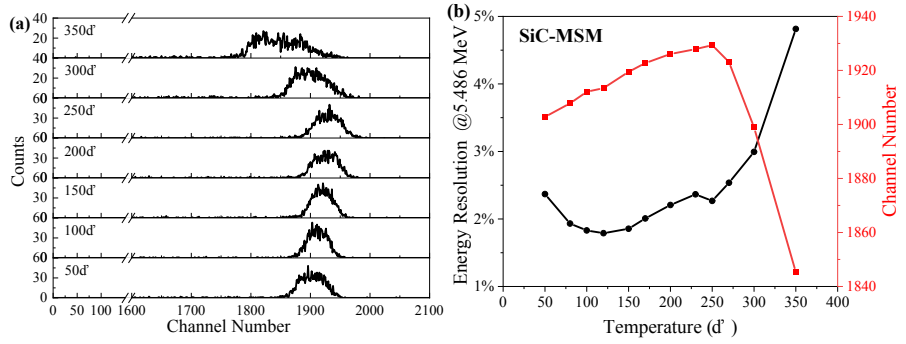


**Fig. 12** (a) PHSs of SiC-MSM device at 50℃-350℃; (b) Energy resolution and peak position

change with temperatures

The PHSs for Diamond-MSM at different temperatures are shown in **Fig.** 13(a). The energy resolution FWHM and peak positions versus temperature curves are shown in **Fig.** 13(b) from 50℃ to 350℃. The data reveal that the energy resolution is optimal at 200°C. From 50°C to 300°C, the energy resolution of the Diamond-MSM detector remains consistently below 2.5%, indicating excellent thermal stability. It is worth noting that even at 350°C, Diamond-MSM devices do not need to reduce the voltage to achieve stable operation. In comparison to 4H-SiC devices, the Diamond-MSM detector demonstrates superior thermal stability and energy resolution. SiC-based detectors, exhibit a notable increase in leakage current and a subsequent deterioration in energy resolution as the temperature rises, especially at higher temperatures (e.g., above 150°C for SiC-MSM and above 300°C for SiC-MSM). In contrast, the Diamond-MSM detector maintains stable performance with an energy resolution consistently below 2.5% across a wider temperature range (up to 350°C), reflecting its robust thermal management. This consistent performance suggests that Diamond-MSM detectors are more reliable for high-temperature applications, where thermal stability is critical. Additionally, the lower energy resolution degradation at elevated temperatures in Diamond-MSM devices highlights their advantages over 4H-SiC detectors in environments with fluctuating or higher temperatures. Overall, Diamond-MSM detectors offer enhanced performance and stability, making them more suitable for a broader range of demanding applications.

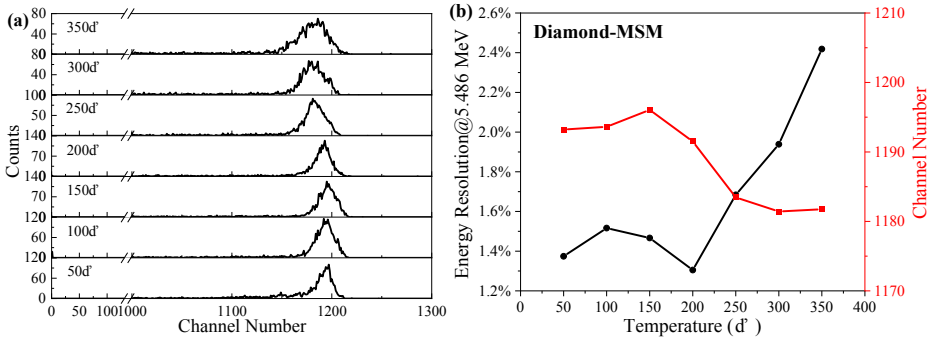


**Fig. 13** (a) PHSs of Diamond-MSM device at 50℃-350℃; (b) Energy resolution and peak position change with temperatures

### 3.3 Fast neutron response

Based on HINEG, the PHS of the SiC-SBD detector under 14.1-MeV neutrons are shown in **Fig.** 14(a). The test was performed at a distance of about 75 cm between the neutron source and detector at 25°C. The spectra were calibrated using the $^{12}C$ (n, $\alpha_0$) $^{9}Be$ reaction correlation peak, corresponding to 8.3 MeV. Below 4 MeV, the response of the SiC detector is dominated by the elastic and inelastic scattering of neutrons on $^{12}C$ and $^{28}Si$ nuclei. At the higher energies, the contribution of charged products produced by $^{12}C$ (n, $\alpha_1$) $^{9}Be$ with a total energy of 6.72 MeV is overshadowed by the $^{12}C$ (n, n') 3α continuum. The strongest peak in the spectrum

appears at 8.3 MeV with an energy resolution of 2.6%, attributed to the $^{12}C$ (n, $\alpha_0$) $^{9}Be$ reaction at the ground state of $^{12}C$. A secondary peak at 11.4 MeV, associated with the same reaction channel in $^{28}Si$, is observed but is less intense compared to the $^{12}C$ peak. This is because the (n, α) reaction in $^{28}Si$ results in the production of $^{25}Mg$ at excited levels, with the corresponding multiple excitation levels identified in **Fig. 14**(a).

For the 14.1 MeV neutron, the reaction cross section for $^{12}C$ (n, $\alpha_0$) $^{9}Be$ reaction is 62.3 mb, and the macroscopic cross section of 4H-SiC is $3.0\times10^{-3}$ $cm^{-1}$. With a neutron flux of $2.78\times10^{8}$ $cm^{-2}$, the total number of reactions is calculated to be 6665 by Eq. (5), which exceeds the actual $^{12}C$ (n, $\alpha_0$) $^{9}Be$ count of 6189. This discrepancy arises because the 8.3 MeV alpha particles, with a range of 36.6 μm in 4H-SiC, escape from the detector's sensitive volume, which has a thickness of 80 μm. The source strength was varied between $2.5\times10^{10}$ n/s, $1.5\times10^{10}$ n/s, $5.0\times10^{9}$ n/s, and $2.0\times10^{9}$ n/s, and the relationship between detector counting rate and neutron source strength was shown in **Fig. 14**(b). The R-square value of the linear fitting curve is 0.99984, demonstrating that the detector's counting rate has an excellent linear relationship with the neutron source intensity.

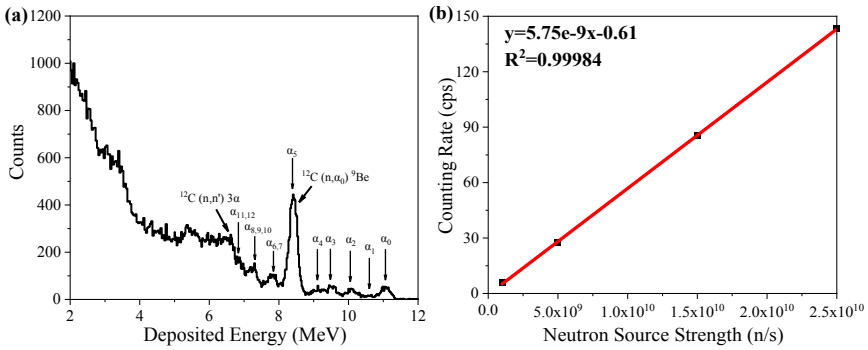


**Fig. 14** (a) PHS of SiC-SBD for 14.1-MeV neutrons at 25℃; (b) Variation of counting rate with neutron source intensity

The PHS of the SiC-MSM detector under 14.1-MeV neutrons are shown in **Fig. 15**(a). The test was performed at a distance of about 80 cm between the neutron source and detector at 25°C. The energy spectrum is basically consistent with that of SiC-SBD as shown in **Fig. 14**(a), but exhibits a worse energy resolution (4.9%@8.3 MeV), which is generally consistent with the results of previous α response tests. When the neutron flux is $1.24\times10^{9}$ $cm^{-2}$, the calculated total number of reactions is 4769, which is higher than the actual $^{12}C$ (n, $\alpha_0$) $^{9}Be$ count 4474. The source strength is set to $1.7\times10^{10}$ n/s, $1.0\times10^{10}$ n/s, $5.6\times10^{9}$ n/s, and $2.1\times10^{9}$ n/s. The relationship between detector counting rate and neutron source strength is shown in **Fig. 15**(b). The R-square value of the linear fitting curve is 0.99888, which indicates that the detector counting rate has good linearity with the neutron source intensity.

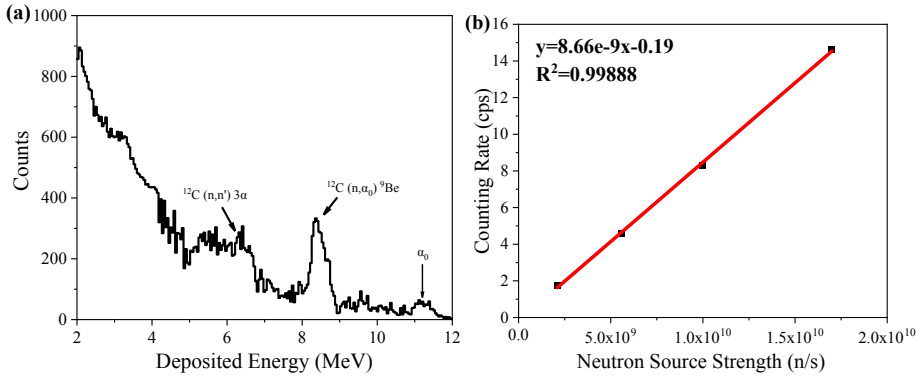


**Fig. 15** (a) PHS of SiC-MSM for 14.1-MeV neutrons at 25℃; (b) Variation of counting rate with neutron source intensity

The PHS of the Diamond-MSM detector under 14.1-MeV neutrons is shown in **Fig.** 16(a). The test was performed at a distance of about 36 cm between the neutron source and detector at 25°C. Below 4 MeV, the elastic and inelastic scattering of the neutrons on $^{12}$C nuclei dominate the response of the Diamond-MSM detector. At higher energies, a well-defined peak due to the $^{12}$C (n, $\alpha_0$) $^9$Be reaction is clearly visible, with an energy resolution of 2.6% at 8.3 MeV. The response of SiC detectors exhibits some peaks due to the reaction between neutron and $^{28}$Si nuclei in the energy range from 7 to 12 MeV which are absent for the diamond. The macroscopic cross section of diamond for $^{12}$C (n, $\alpha_0$) $^9$Be is calculated as $1.1\times10^{-2}$ cm$^{-1}$. With a neutron flux of $4.13\times10^8$ cm$^{-2}$, the calculated total number of reactions is 29278, which closely matches the $^{12}$C (n, $\alpha_0$) $^9$Be count of 29131 observed in the actual test. For the same neutron flux and detection area, the counting rate for the $^{12}$C (n, $\alpha_0$) $^9$Be peak in the diamond is 24.6 times higher than that in 4H-SiC. This significant difference is attributed to the higher carbon atomic density and the thicker sensitive region of the diamond detector compared to the SiC detectors. The source strength was varied between $1.0\times10^{10}$ n/s, $5.7\times10^9$ n/s, $3.0\times10^9$ n/s, and $1.2\times10^9$ n/s, and the relationship between detector counting rate and neutron source strength for the Diamond-MSM is shown in **Fig.** 16(b). The R-squared value of the linear fitting curve is 0.99921, indicating that the detector's count rate is highly linear with the neutron source intensity.

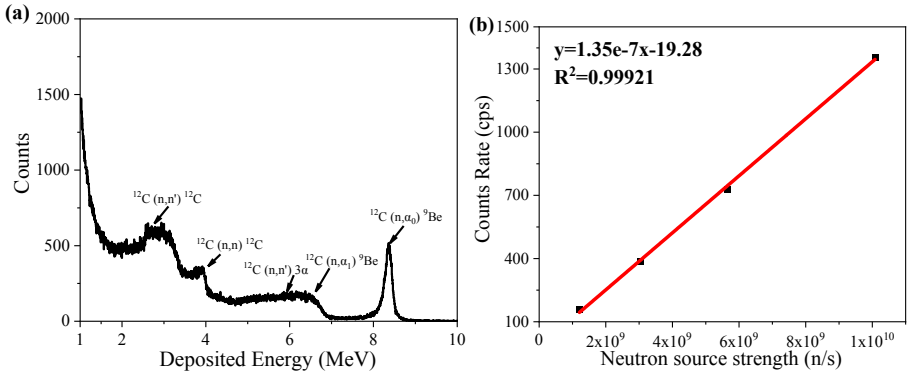


**Fig. 16** (a) PHSs of Diamond-MSM device for 14.1 MeV at 25℃; (b) Variation of counting rate with neutron source intensity

## 4 Conclusion

In this study, we systematically compared the performance of 4H-SiC, SiC-MSM, and Diamond-MSM detectors under high-temperature and radiation environments, focusing on their I-V characteristics, alpha particle response, energy resolution, and fast neutron detection capabilities. Our results provide critical insights into the stability and performance of these semiconductor materials under extreme conditions.

The I-V characteristics of SiC-SBD, SiC-MSM, and Diamond-MSM were evaluated at elevated temperatures to assess their thermal stability. For SiC-SBD, a significant temperature dependence of the reverse leakage current was observed. At 25°C, the leakage current was 3.21 nA, which increased to 5.35 μA at 200°C. This indicates that the SiC-SBD exhibits high leakage current and poor thermal stability at higher temperatures. In contrast, the SiC-MSM showed better thermal stability, with the leakage current increasing from 0.57 nA at 25°C to 91.75 nA at 350°C, indicating a slower rise in leakage current compared to the SiC-SBD. The leakage current in the Diamond-MSM detector showed the least variation with temperature. At 25°C, the leakage current was less than 1 nA, and even at 350°C, it remained below 5 nA, demonstrating its excellent high-temperature stability. These results highlight that the MSM structure offers superior thermal stability compared to the SBD structure, and that high-temperature degradation of the dark current of Diamond-MSM detector is better than SiC counterpart. In terms of α-particle response, the SiC-SBD achieved an energy resolution of 0.61% at 5486 keV at room temperature, while the energy resolutions for SiC-MSM and Diamond-MSM were 1.21% and 0.97%, respectively. Regarding α-particle response in high-temperature environments, SiC-SBD is suitable for use in environments up to 150°C, SiC-MSM is suitable for environments up to 300°C, and Diamond-MSM is suitable for environments up to 350°C and beyond. Compared to SiC devices, Diamond-MSM device demonstrates excellent stability under high-temperature conditions. For fast neutron response, all three detectors show good linearity and high counting rate. Diamond has a high carbon atom density and exhibits the best neutron detection sensitivity. The energy resolutions of SiC-SBD, SiC-MSM, and Diamond-MSM for 8.3 MeV are 2.6%, 4.9%, and 2.6%, respectively.

In summary, SiC-SBD devices have the advantage of precise detection in low-temperature environments, while both SiC-MSM and Diamond-MSM devices are capable of meeting the high-temperature operating requirements of the CFETR.

## Acknowledgements

This work was supported by the Project of the National Research and Development Program for Major Research Instruments of China (No. 62027814), the Joint Funds of the National Natural Science Foundation of China (No. U2436201), by National Natural Science Foundation of China (Nos. 62134006, 62204193, and 62421005), the China Postdoctoral Science Foundation (No. 2021TQ0256), Anhui Provincial Major Science and Technology Project (Nos. E35AH205B3 and E35AH205B4) and the Anhui Province Ecological Environment Research Project (No. 2023hb0017). The authors would like to express their gratitude for the technical support on the

radiological test system from the Institutional Center for Shared Technologies and Facilities of the Institute of Nuclear Energy Safety Technology, Hefei Institutes of Physical Science, Chinese Academy of Sciences, Hefei, China.

## References

[1] W. Tong, H. Li, M. Xu et al., Neutron irradiation influence on high-power thyristor device under fusion environment. Nuclear Science and Techniques. **35(4)**, 72-88 (2024). https://doi.org/10.1007/s41365-024-01433-1

[2] W. Zhou, X. Fang, J. Fang et al., Numerical and experimental analysis of AC loss for CFETR CS model coil. Nuclear Science and Techniques. **28**, 1-8 (2017). https://doi.org/10.1007/s41365-017-0301-0

[3] H. Xiong, Q. Zeng, Y. Han et al., Neutronics analysis of a subcritical blanket system driven by a gas dynamic trap-based fusion neutron source for 99Mo production. Nuclear Science and Techniques. **34**, 1-12 (2023). https://doi.org/10.1007/s41365-023-01206-2

[4] L. Ren, Y. Han, X. Meng et al., Effect of NO annealing on radiation detection performance of Ni/SiO2/4H-SiC MOS capacitors. Nuclear Instruments and Methods in Physics Research A. **1070**, 170073 (2025). https://doi.org/10.1016/j.nima.2024.170073

[5] P. Hu, L. Xu, S. Zhang et al., Failure mechanisms of AlGaN/GaN HEMTs irradiated by high-energy heavy ions with and without bias. Nuclear Science and Techniques. **36(1)**, 1-10 (2025). https://doi.org/10.1007/s41365-024-01567-2

[6] D. Szalkai, R. Ferone, F. Issa et al., Fast neutron detection with 4H-SiC based diode detector up to 500 °C ambient temperature. IEEE Transactions on Nuclear Science. **63(3)**, 1491-1498 (2016). https://doi.org/10.1109/TNS.2016.2522921

[7] S. Tripathi, C. Upadhyay, C. Nagaraj et al., Investigation of enhancement in planar fast neutron detector efficiency with stacked structure using Geant4. Nuclear Science and Techniques. **28**, 1-10 (2017). https://doi.org/10.1007/s41365-017-0315-7

[8] G. Grin, C. Joseph, C. Wong et al., Scattering of 14.1MeV neutrons from 12C. Physics Letters B. **25(6)**, 387-390 (2016). https://doi.org/10.1016/0370-2693(67)90153-0

[9] P. Xu, Y. Yu, H. Zhou. Fabrication of single-crystal diamond neutron detector and its application in 14.1 MeV neutron detection in deuterium-tritium fusion experiment. Plasma Science and Technology. **25(7)**, 075101 (2023). https://doi.org/10.1088/2058-6272/acb48a

[10] M. Rebai, D. Rigamonti, S. Cancelli et al., New thick silicon carbide detectors: Response to 14 MeV neutrons and comparison with single-crystal diamonds. Nuclear Instruments and Methods in Physics Research Section A. **946**, 162637 (2019). https://doi.org/10.1016/j.nima.2019.162637

[11] G. Cheng, Y. Chen, L. Yan et al., PL and ESR study for defect centers in 4H-SiC induced by oxygen ion implantation. Nuclear Science and Techniques. **28**, 1-6 (2017). https://doi.org/10.1007/s41365-017-0263-2

[12] F. Ruddy, A. Dulloo, J. Seidel et al., The fast neutron response of 4H silicon carbide semiconductor radiation detectors. IEEE Transactions on Nuclear Science. **53(3)**, 1666-1670 (2006). https://doi.org/10.1109/TNS.2006.875151

[13] D. Rigamonti, L. Giacomelli, G. Gorini et al., Neutron spectroscopy measurements of 14 MeV neutrons at unprecedented energy resolution and implications for deuterium–tritium fusion plasma diagnostics. Measurement science and technology. **29(4)**, 045502 (2018).

https://doi.org/10.1088/1361-6501/aaa675
[14] O. Obraztsova, L. Ottaviani, A. Klix et al., Comparing the response of a SiC and a sCVD diamond detectors to 14-MeV neutron radiation. IEEE Transactions on Nuclear Science. **65(9)**, 2380-2384 (2018). https://doi.org/10.1109/TNS.2018.2848469.1
[15] D. Szalkai, R. Ferone, F. Issa et al., Fast neutron detection with 4H-SiC based diode detector up to 500°C ambient temperature. IEEE Transactions on Nuclear Science. **63(3)**, 1491-1498 (2016). https://doi.org/10.1109/TNS.2016.2522921
[16] T. Shimaoka, S. Koizumi, J. Kaneko. Recent progress in diamond radiation detectors. Functional Diamond. **1(1)**, 205-220 (2022). https://doi.org/10.1080/26941112.2021.2017758
[17] Y. Liu, J. Lu, X. Li et al., A 4H–SiC betavoltaic battery based on a 63Ni source. Nuclear Science and Techniques. **29(11)**, 60-68 (2018). https://doi.org/10.1007/s41365-018-0494-x
[18] L. Ren, R. Li, Y. Han et al., High performance 4H-SiC detectors for superheavy elements study. Nuclear Instruments and Methods in Physics Research Section A. **1072**, 170181 (2024). https://doi.org/10.1016/j.nima.2024.170181
[19] K. Mandal, J. Kleppinger, S. Chaudhuri. Advances in high-resolution radiation detection using 4H-SiC epitaxial layer devices. Micromachines. **11(3)**, 254-267 (2020). https://doi.org/10.3390/mi11030254
[20] I. Kulagin, M. Li, V. Laitinen et al., Review of MSM actuators: applications, challenges, and potential. IEEE Access. **10**, 83841-83850 (2022). https://doi.org/10.1109/ACCESS.2022.3197278
[21] T. Shimaoka, J. Kaneko, Y. Arikawa et al., Measurement of neutrons produced by inertial fusion with a diamond radiation detector. Sensors & Materials. **36(1)**, 217-223 (2024). https://doi.org/10.18494/SAM4671
[22] L. Ren, Y. Han, J. Zhang et al., Neutronics analysis of a stacked structure for a subcritical system with LEU solution driven by a D-T neutron source for 99Mo production. Nuclear Science and Techniques. **32(11)**, 1-11 (2021). https://doi.org/10.1007/s41365-021-00968-x
[23] W. Cheng, K. Deng, Y. Zeng et al., Development of an enhanced online tritium monitoring system using plastic scintillation fiber array. Nuclear Science and Techniques. **35(10)**, 173-185 (2024). https://doi.org/10.1007/s41365-024-01518-x
[24] S. Chen. Low-energy atomic displacement model of SRIM simulations. Nuclear Science and Techniques. **32(11)**,1-10 (2021). https://doi.org/10.1007/s41365-021-00971-2.
[25] Y. Ding, Y. Nie, Y. Zhang et al., Benchmark experiment on slab (238)U with D-T neutrons for validation of evaluated nuclear data. Nuclear Science and Techniques. **35(2)**, 145-159 (2024). https://doi.org/10.1007/s41365-024-01386-5
[26] S. Ding, J. Zhang, K. Su et al., Single-crystal diamond grown through high-power-density epitaxy used for a high-performance radiation detector. Science China Materials. **67(7)**, 2329–2334 (2024). https://doi.org/10.1007/s40843-024-2955-x
[27] K. Su，H. Wang，Q. He et al., A large gain and high resolution diamond radiation detector With Au/Hydrogen termination ohmic contact. IEEE Electron Device Letters. **43(3)**, 454-457 (2022). https://doi.org/10.1109/LED.2022.3145241
[28] K. Su, Z. Ren, J. Zhang et al., High performance hydrogen/oxygen terminated CVD single crystal diamond radiation detector. Applied Physics Letters. **116**, 092104 (2020). https://doi.org/10.1063/1.5135105

[29] F. Wang, B. Hong, T. Li et al., Feasibility study on fast neutron yield measurement with 4H-SiC detector. Nuclear Science and Techniques. **44(6)**, 6-15 (2022). **(in Chinese)**

[30] H. Umezawa, S. Shikata. Leakage current analysis of diamond Schottky barrier diodes operated at high temperature. Japanese Journal of Applied Physics. **53(4S)**, 04EP04 (2014). https://doi.org/10.7567/JJAP.53.04EP04

[31] N. Gál, L. Hrubčín, A. Šagátová et al., High-resolution alpha-particle detector based on Schottky barrier 4H-SiC detector operated at elevated temperatures up to 500℃. Applied Surface Science. **635**, 157708 (2023). https://doi.org/10.1016/j.apsusc.2023.157708